Confined Synthesis and Integration of Functional Materials in Sub-nanoliter Volumes

Benjamin Z. Cvetković,[†,§] Josep Puigmartí-Luis,[†,§] Daniel Schaffhauser,[†] Thomas Ryll,[‡] Stefan Schmid,[†] and Petra S. Dittrich[†,*]

[†]Department of Chemistry and Applied Biosciences and [‡]Department of Materials, ETH Zurich, 8093 Zurich, Switzerland. [§]These authors contributed equally to this work.

ABSTRACT We present a novel microchip-based approach to combine the synthesis, characterization, and utilization of different functional materials on a single platform. A two-layer microfluidic device comprising 10 parallel actuated reaction chambers with volumes of a few hundred picoliters is used to localize and confine the synthesis, while the surfaces of the reaction chambers comprise an electrode array for direct integration and further characterization of the created crystalline assemblies without the need for further manipulation or positioning devices. First we visualized and evaluated the dynamics of our method by monitoring the formation of a fluorescent metal–organic complex (Zn(bix)). Next, we induced the site-specific growth of two types of organic conductive crystals, AuTTF and AgTCNQ, directly onto the electrode arrays in one- and two-step reactions, respectively. The performance of the created AgTCNQ crystals as memory elements was thoroughly examined. Moreover, we proved for first time that AuTTF composites can be used as label-free sensing elements.

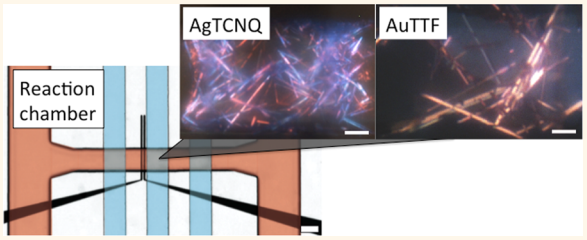

KEYWORDS: microreactor chamber · functional materials · charge transfer · diffusive mixing · sensors

The formation of complex functionalized nano- and micrometer-sized structures requires both specific precursors and well-defined assembly pathways to allow reproducible organization of the molecular units. In particular, materials in the crystal state are highly desired for their high molecular order, which can easily favor functionality. For example, in organic electronics, it has been demonstrated that a defect-free molecular order is required to greatly increase the performances of crystals and films, thus improving device application and function.[1−5] However, it is difficult to identify optimum conditions for crystallization and to reproduce these conditions in a controlled environment. Furthermore, high accuracy during assembly and deterministic positioning of functional nanostructures are essential requirements for their integration into usable devices operating with optimum performance.[6−8]

Conventional techniques to form assemblies in the nanometer dimension include purely chemical synthetic approaches,[9−16] vapor deposition,[17−20] and electrochemical processes.[21] Positioning of nanostructures during their assembly became possible by patterning of nucleation sites.[18,20,22,23] For example, dip-pen nanolithography has been used to control the initiation and kinetics of polymer crystal growth.[24,25] More recently, a dip-pen direct delivery of femtoliter reagent volumes enabled the submicrometer crystallization of metal–organic complexes at desired locations on a surface.[23] However, the solubility and diffusion of small molecules together with control over the drying conditions remain some of the hurdles of this technique.

In recent years, microfluidics has been proven to be a particularly attractive method for the formation of nanostructures because the technology provides superior opportunities for fluid handling and metering, which enables precise spatial localization of small reagent volumes.[26−32] The turbulence-free laminar flow pattern in microfluidic devices facilitates the prediction of molecular concentration distributions with respect to their diffusion coefficients, which enable reaction at predefined places, *e.g.*, at very well-defined interfaces of co-flowing streams,[30,33−35] and can be combined with electrochemical methods.[36]

* Address correspondence to dittrich@org.chem.ethz.ch.

Received for review August 10, 2012 and accepted December 4, 2012.

Published online December 04, 2012
10.1021/nn303632n

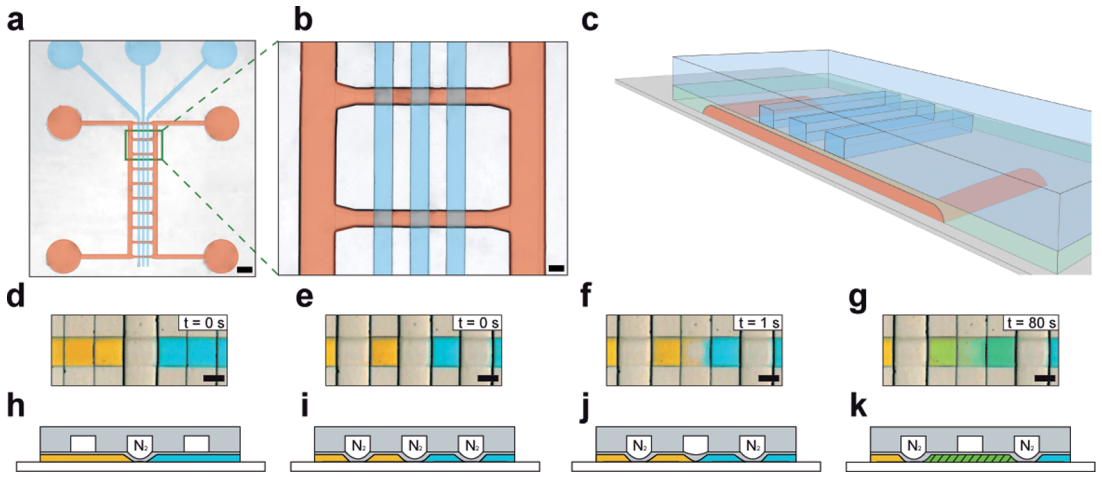

Figure 1. Design and operation of the device made in PDMS by multilayer soft lithography. (a) Micrograph of the multilayer PDMS chip with an array of 10 parallel microchambers in the fluid layer (red channels, 10 μm high). Fluid metering and supply is controlled by three pneumatically actuated valves (control layer, blue channels, 100 μm high). Scale bar: 750 μm. (b) Magnification of two microchambers. The final microchambers are confined by the two side valves and encapsulate a volume of 675 pL. Scale bar: 150 μm. (c) 3-D schematic view of one microchamber (not to scale). (d–g) Series of micrographs showing the operation of the valves and the diffusive mixing of two food dyes in a typical reaction procedure. (d) Introduction of the reagents, (e) compartmentalization of two reagent volumes on either side, (f) opening of the central valve, and (g) diffusive mixing. Scale bars: 100 μm. (h–k) Corresponding schematic side views.

Furthermore, chemical reactions confined in nanoliter and sub-nanoliter volumes within microfluidic platforms have been reported using microwells created in glass or polymer surfaces[37–39] or within water-in-oil droplets.[40–42] Continuous, droplet-based methods are useful to rapidly screen reaction conditions and to systematically vary the concentration of precursors. However, some aspects such as the conductance of multistep reactions, solvent exchange, the washing steps, and the separation of the product from the oil phase remain challenging. For the formation of nanostructures, the further integration into a functional unit remains difficult. Alternatively, micrometer-sized reactor chambers can be created by integrating pneumatically or hydrodynamically actuated valves into microfluidic channel networks. These static microreactors can be arranged in a highly parallel fashion and used for biochemical and chemical reactions.[43] For example, Quake and co-workers reported a microdevice where two separate volumes could be merged together under convection-free conditions.[44,45] The microchip was used for screening the optimum conditions for protein crystallization.

Here, we adopted this approach and optimized it for the localized formation of metal–organic-based materials. We employ microchamber arrays, each encapsulating a volume of a few hundred picoliters, to form anisotropic structures ("micro- and nanowires") in one- or two-step reactions under mild conditions. This localized formation opens the door to directly use and characterize the structures by means of integrated microelectrodes patterned on the surface of the microchambers and connected to external readout devices. Moreover, we demonstrate the ability of the conductive wires for sensing of vaporized solvents.

RESULTS AND DISCUSSION

The microfluidic device was fabricated using standard soft lithography methods and consists of two layers (Figure 1), one bottom layer for fluid supply (hereafter referred to as the fluid layer) and a top layer for pneumatic actuation of the integrated valves (hereafter referred to as the control layer; for further details see Experimental Section). The platform implements 10 parallel microchambers operated by three parallel control lines. Upon pressurization with nitrogen, a polydimethylsiloxane (PDMS) membrane is lowered into the chamber to form tightly closing valves. In a typical experiment, two reagents are supplied from either side of the microchip into the microchambers, while the central valve is closed. Actuation of the outside valves on both sides results in the compartmentalization of the two reagents into a precise volume of 300 or 675 pL, depending on the microchip design. Once the middle valve is opened, the two liquids are in contact, allowing diffusion of the precursors within the microchamber. The operation of the device is visualized in Figure 1d–g using two food dyes together with schematic side-view representations of the entire diffusive process, as shown in Figure 1h–k. Undoubtedly, a completed diffusion mixing was manifested with the appearance of green color in the entire microreaction chamber after yellow and blue food dyes were allowed to spread within the enclosed and localized reaction volume (Figure 1g). Additionally studies were performed with fluorescent beads to demonstrate and ensure the diffusive mixing

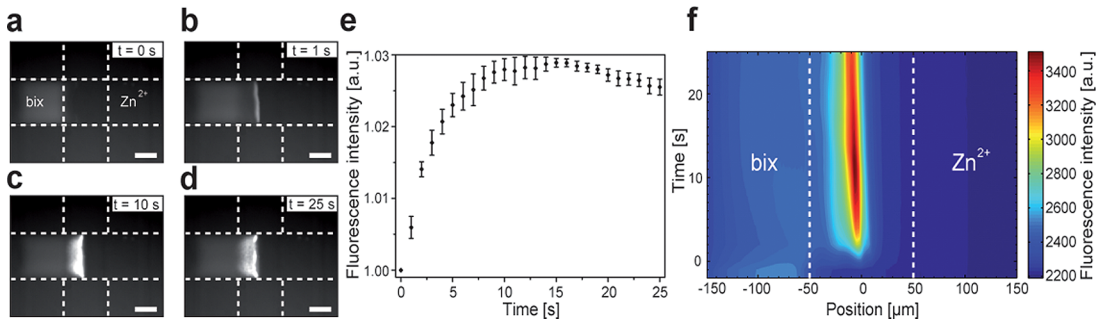

Figure 2. Formation of the fluorescent metal organic complex Zn(bix). (a–d) Fluorescence images taken at different times after opening the central valve. Scale bars: 50 μm. (e) Normalized fluorescence intensity of the microchambers *versus* time. The values are averages of four measurements. The reaction was completed after about 10 s. (f) 2-D surface plot of the time-resolved reaction showing the fluorescence intensity within the microchamber.

condition of the device (see Supporting Information movie M1).

Next, we visualized the interface by the localized synthesis of a metal–organic complex, Zn(bix), based on the coordination between zinc metal ions and 1,4-bis(imidazol-1-ylmethyl)benzene (bix) molecules. This complex was selected as it exhibits a strong blue fluorescence after coordination of zinc metal ions with bix molecules.[46] To induce the reaction, an aqueous solution of $Zn(NO_3)_2$ (20 mM) and a solution of bix in ethanol (20 mM) were supplied to the microchamber while keeping the middle valve closed. After compartmentalization and opening of the middle valve, the reaction occurred immediately. Figure 2a–d shows a sequence of fluorescence images monitoring the reaction inside the microchamber at different times. Image analysis of the fluorescence intensity over the course of the coordination reaction at the interface suggests a complete coordination within 10 seconds (Figure 2e). Note that the interface is blurred toward the compartment where bix was initially introduced, because Zn ions diffuse much faster toward this compartment, thereby reacting with the slower diffusing bix molecules. Such precise confinement of a reaction is almost impossible to achieve in a conventional synthetic process and may allow mechanistic studies of mixing, complexation, and coordination processes.

Having this tool for localized synthesis, we are not only able to form functional materials but can also directly integrate the structures with electric readout components without any further manipulation processes, which could harm their quality and function. For this, the microfluidic system was sealed to a glass plate that was patterned with an electrode array matching the design of the microchambers so that each chamber contained a pair of electrodes (Supporting Information Figure S1). These electrodes were connected *via* conventional wires to external instruments. In the following, we show the synthesis and characterization of conductive crystalline structures made of metal–organic compounds either by a solid-state reaction (AgTCNQ) or in solution (AuTTF) (Supporting Information, Figures S2 and S3, respectively).

AgTCNQ crystal growth required a two-step reaction process. First, a controllable growth of silver layers inside 10 parallel microchambers was performed by the reaction of silver salt solution (AgX) with reducer agent solution (ReD) (Figure 3a (i) and 3b). After rinsing off the surplus solution, the chip was dried and saturated tetracyanoquinodimethane (TCNQ) solution in acetonitrile was added to the reaction chamber, keeping one of the side valves closed to allow only diffusion of TCNQ into the microchamber (Figure 3a (ii) and Supporting Information Figure S4). Formation of AgTCNQ wires could be observed within a few minutes, and after total consumption of the electroless-deposited silver layer, the TCNQ residue was washed away with pure acetonitrile (Figure 3a (iii)).

The deterministic positioning of the silver film in the first reaction step inside the microreactor chambers enabled the site-specific growth of crystalline AgTCNQ structures in the second reaction step. Electroless deposition of silver has been previously demonstrated within microfluidic platforms for fluidic-assisted formation of silver wires;[33,47] however the on-chip chemical conversion into AgTCNQ is novel. It is especially attractive because it constitutes a promising example toward localized multistep synthesis and solid-state reactions in sub-nanoliter volumes. In addition, AgTCNQ structures could be used as a crystalline scaffold for the fabrication of organic memories and logic molecular electronic components.[14,16,21,48–52]

Optical images of the microchambers observed with a polarized light microscope clearly indicate the formation of AgTCNQ crystals with anisotropic, wire-like morphology (Figure 3c,d and Supporting Information Figure S5). The AgTCNQ wire-like crystals are not perfectly uniform in size. Typically, diameters ranging from 1 to 1.5 μm and lengths from 7 to 50 μm were characterized from a statistical treatment of optical micrographs collected from repeated experiments. This random size distribution may result from different silver film thickness, as demonstrated previously with

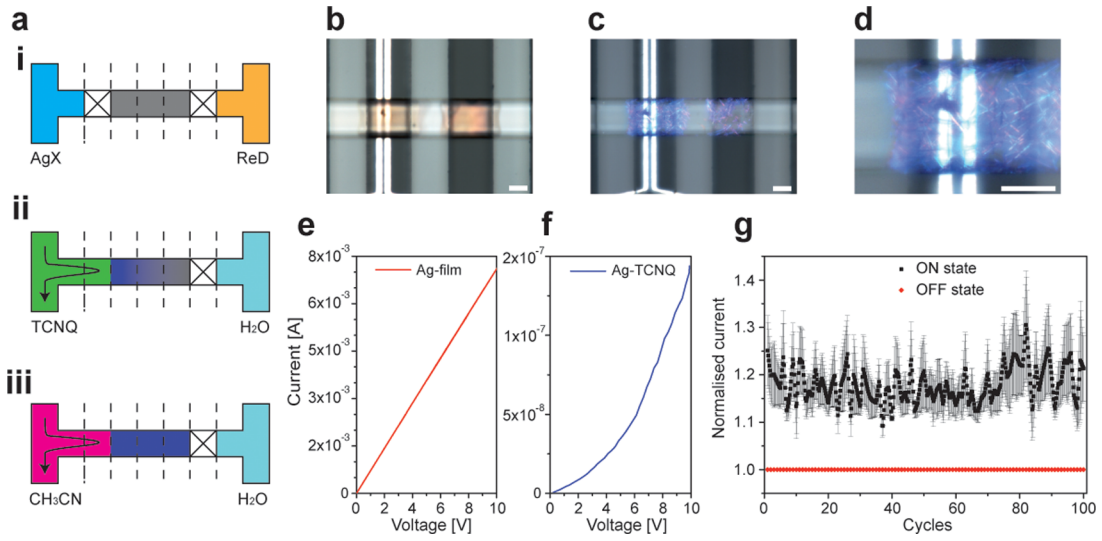

Figure 3. (a) From (i) to (iii) schematic illustrations showing the AgTCNQ wire formation inside a microreactor chamber. (b) Micrograph of an *in situ* formed silver layer inside a microreactor chamber. (c) Polarized micrograph of the same microchamber after reaction with saturated TCNQ solution in acetonitrile, and (d) a magnified image of (c). In white, platinum electrodes patterned on top of the glass slide (electrode height: 100 nm). (e and f) Representative *I*−*V* characteristics of a silver film and AgTCNQ wires formed inside a microfluidic platform, respectively. (g) Graph showing the averaged normalized current (I_{ON}/I_{OFF}) in the ON-OFF state of on-chip-formed AgTCNQ memory as a function of the number of cycles. The data presented correspond to three distinct microreaction chambers. The voltage considered for the ON-OFF state plotting was fixed at 8 V. Scale bars: 50 μm.

vacuum deposited metal films.[20,50,53] Optical microscopy images and scanning electron microscopy studies performed at different silver film thicknesses and at lower silver precursor concentrations verified this assumption (Supporting Information Figures S6 and S7).

The AgTCNQ crystals were characterized by attenuated total reflectance (ATR) IR spectroscopy, powder X-ray diffraction (PXRD), scanning electron microscopy (SEM), and energy dispersive X-ray spectroscopy (EDX). SEM-EDX studies confirmed the presence of Ag, N, and C in the AgTCNQ wires (Supporting Information Figure S8), and ATR-IR spectroscopy indicated characteristic peaks of AgTCNQ with bands assigned to reduced TCNQ molecules located at 2198, 2183, 2160, 1506, and 822 cm^{-1} (Supporting Information Figure S9a).[13,54,55] PXRD characterization confirmed the crystalline nature of the AgTCNQ wires, and the presence of peaks at 2θ = 10.3°, 14.6°, 20.3°, 20.8°, 21.2°, 23.0°, and 23.5° proved the formation of AgTCNQ crystals in the form of AgTCNQ phase II (Supporting Information Figure S9b).[10,11,51]

To confirm the success of the direct integration of AgTCNQ wires, electrical characterization of the silver layer before and after reaction with saturated TCNQ solution was performed following solvent evaporation at room temperature and under ambient conditions. Figure 3e presents a linear *I*−*V* sweep of the silver film, which indicates its metallic character and good contact with the microfabricated electrodes, and a nonlinear symmetric curve from the AgTCNQ wires produced after the on-chip conversion (Figure 3e and f, respectively). By applying a reversible electric field, two switchable states were confirmed, indicating low (or OFF) and high (or ON) conductivity states. These memory effects of AgTCNQ wires have been observed by other groups in former studies and are potentially useful for electronic devices.[16,19,20] Noteworthy, no degradation in the wires' performance was observed even after 100 cycles (Figure 3g and Supporting Information Figure S10).

The second synthesis was the formation of crystalline AuTTF wires, which was initiated after static compartmentalization of tetrathiafulvalene (TTF, 24 mM) and hydrogen tetrachloroaurate (6 mM) solutions, both in acetonitrile, and subsequent release of the middle valve (Supporting Information Figure S11). Lower concentrations resulted in no visible wire formation (data not shown), thus suggesting an optimized range of concentrations to be used in order to guarantee a rapid and visible synthesis of AuTTF wires inside the microreaction chambers. Figure 4a shows a polarized micrograph of AuTTF wires formed in the microchamber synthesis. Micrographs acquired through crossed polarizers indicate the crystalline nature of the AuTTF wire-like structures (Supporting Information Figure S12). *I*−*V* characteristics were studied with the two-point probe method after acetonitrile was evaporated at room temperature. Several AuTTF wires were measured after formation inside different microchambers showing similar *I*−*V* dependencies (Figure 4b). The uniformity of these results demonstrates the suitability of the method for parallelized integration.

Nano- and micrometer-sized conductive wires could potentially be used as highly sensitive sensors. We proved the AuTTF sensing capabilities upon direct

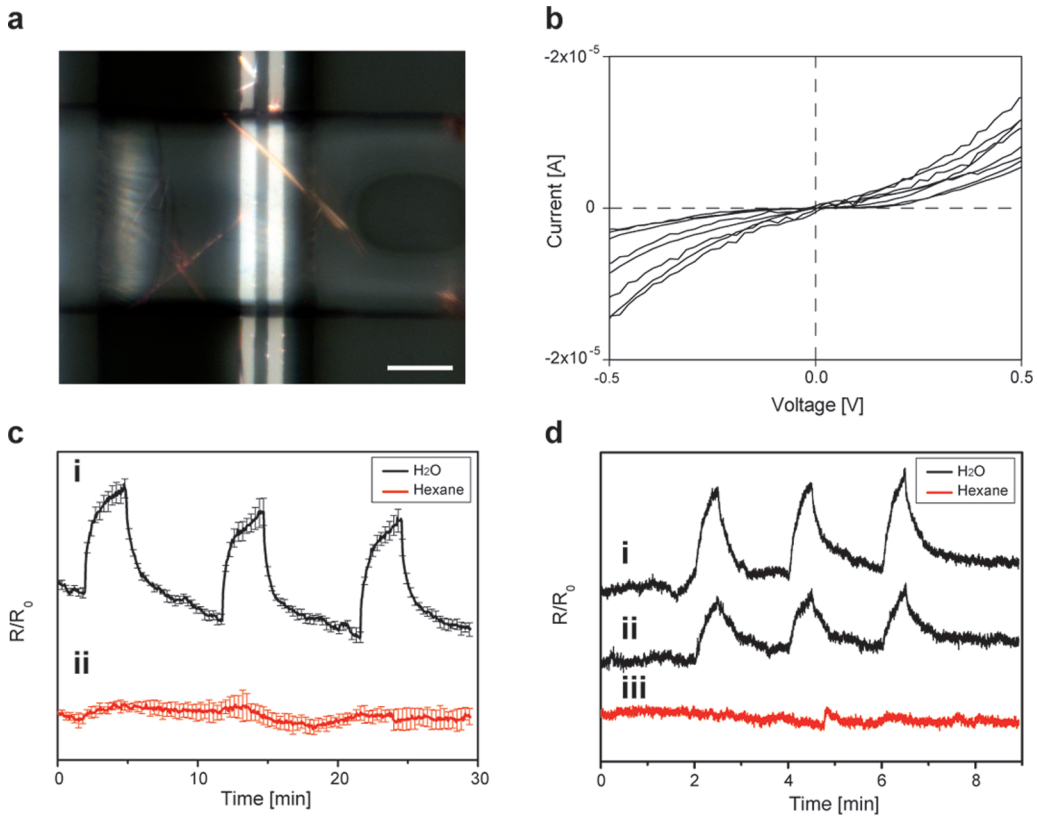

Figure 4. Formation and electric characterization of AuTTF wires and sensing performance. (a) Polarized micrograph of AuTTF wires formed inside a microrector chamber and (b) multiple *I*−*V* sweeps of different integrated AuTTF wires. (c) Normalized resistance response of five different AuTTF sensing elements cycled between (i) dry nitrogen gas and water vapors and (ii) dry nitrogen gas and hexane vapors (exposure times: 3 min). (d) Normalized resistances of one AuTTF sensing element exposed to (i) three injections of water (exposure times: 30 s), (ii) three injections of water after more than 30 subsequent injections (exposure times: 30 s), and (iii) three injections of hexane (exposure times: 1 min). All injections in (d) were started at the same time points. Scale bar: 50 μm.

exposure to water and hexane vapors. Electronic transport properties of AuTTF wires were acquired in two- and four-point configuration while exposing them to water and hexane vapors inside a gas-phase chamber regulated with nitrogen gas and a syringe pump system. Normalized resistances of AuTTF sensing elements as a function of time using two- and four-point configuration are shown in Figure 4c and d, respectively. Figure 4c shows averaged normalized resistances of five different AuTTF sensors upon three subsequent exposures to (i) water and (ii) hexane vapors. The injections were performed at equal times and for 3 min in both cases. Experiments conducted under shorter injection times (30 s) confirmed the reversibility and the rapid response of AuTTF sensors to water vapors, even after more than 30 subsequent injections (Figure 4d (i) and (ii)). AuTTF sensing elements were still functional under the conditions investigated. But under sufficient water supply, one may expect shorter lifetimes due to deterioration of the AuTTF wires.

Compared to water vapors, the resistance change induced by hexane vapors was negligible under equal experimental conditions (*e.g.*, exposure times, temperature, humidity, nitrogen and sample infusion flow rates) (Figure 4c (ii)) or longer exposure times (Figure 4d (iii)). These results can be attributed to the lack of interaction between nonpolar molecules and ionic species such as AuTTF charge-transfer salt. In accordance with common understanding, the variation in AuTTF resistance upon exposure to water vapors might be explained by considering noncovalent interactions of water molecules with the cation and anion layer of the AuTTF charge-transfer salt. AuTTF micro- and nanowires are known to have a backbone scaffold of TTF cation radicals stabilized with chloride counterions,[12,34] and hence, it is expected that exposure to water vapor of AuTTF wires will bring variations to the charged components that are directly involved in the current flow of the AuTTF conductive system. Indeed, humidity sensors described from polyelectrolyte materials are based on this principle.[56] While several humidity sensors have been described exploiting resistance or capacitive changes occurring on the surface of ceramics[57,58] or polymer materials,[59−62] the choice of a hybrid charge-transfer salt as a label-free sensing unit opens up new opportunities toward electronic noses and other sensing elements. To the best of our knowledge, this is the first time that AuTTF

composites have been used as sensing elements. Ongoing research in our group is aimed at developing and evaluating a wide range of other volatile substances that could significantly influence the electronic state of AuTTF wires.

CONCLUSION AND OUTLOOK

In summary, this study presents a novel and convenient approach where microchambers enclosing picoliter volumes have been designed to facilitate reactions in predefined small areas of a chip. Furthermore, *in situ* formed functional assemblies were integrated with electrode arrays for direct characterization and application, thus avoiding complex postprocessing or further fabrication steps, which could disrupt their crystal nature. Besides the fine control regarding positioning of functional crystalline materials and their integration, this approach also offers other attractive possibilities. For example, reaction conditions can easily be optimized due to the rapid supply and exchange of reactants and solvents. The combination of reaction-controlled environments and direct integration of functional crystalline assemblies on a surface makes this microfluidic approach an attractive choice for the preparation and investigation of different kinds of organic-based molecular conductors and transistors on a single surface. In other words, this approach could readily provide the basis toward straightforward screening platforms and multifunctional array fabrication with great promise for future work in outstanding disciplines covering molecular electronics, sensors, and optics.

EXPERIMENTAL SECTION

Masters and Multilayer Chip Fabrication. *Fluidic Layer Master Mold Fabrication.* The master mold for the fluidic channel was prepared using a two-inch silicon wafer. First, the silicon wafer was dehydrated for 5 min at 180 °C on a hot plate. After drying, 1 mL of hexamethyldisilazane (Merck) was spin-coated at 7500 rpm for 30 s to increase the adhesion of the photoresist. Next, 1−2 mL of positive photoresist AZ-9260 (Microchemicals) was spin-coated at 1900 rpm during 60 s, creating a resist thickness of approximately 12−13 μm for the fluidic layer. After a soft bake process performed at 110 °C on a hot plate for 200 s, the wafer was exposed to 750 mJ/cm^2 UV light (at 365 nm) using a mask aligner (MA-6 mask aligner, Karl Süss) and a transparency photomask (Circuitgraphics). Development was conducted in a mixture of 25 vol % AZ-400K developer concentrate (Microchemicals) and 75 vol % DI-water for 3−4 min. A reflow of the photoresist at 120 °C during 2 min permitted the formation of round-shaped channels needed for the experiments. Silanization using 1*H*,1*H*,2*H*,2*H*-perfluorodecyldimethylchlorosilane (ABCR) of the final wafer prevented polydimethylsiloxane adhesion during molding of the fluid layers.

Control Layer Master Mold Fabrication. A four-inch silicon wafer was dehydrated at 180 °C on a hot plate for 5 min. Afterward, negative photoresist SU-8 2050 (Microresist) was spin-coated at 1500 rpm for 30 s to create 50 μm high channels, and the wafer was soft baked at 65 °C for 180 s then 450 s at 95 °C on a hot plate. Next, the wafer was exposed to 180 mJ/cm^2 UV light (at 365 nm) using a mask aligner (MA-6 mask aligner, Karl Süss) and a transparency photomask (Circuitgraphics). A postexposure bake was performed for 60 s at 65 °C and then at 95 °C for 420 s on a hot plate. Development was preformed using mr-Developer-600 (Microresist) for 6 min. Finally, the control layer master mold was silanized using 1*H*,1*H*,2*H*,2*H*-perfluorodecyldimethylchlorosilane (ABCR) in order to avoid PDMS adhesion during chip fabrication.

Multilayer Chip Assembly. The multilayer chips were prepared following the protocol established by the Quake group[43] with minor variations. Briefly, a degassed PDMS mixture (20:1 w/w, elastomer/curing agent) was spin-coated at 2300 rpm on the structured two-inch fluidic master mold wafer to create a 12−13 μm high PDMS membrane. The silicon wafer with the spin-coated PDMS layer was then precured for 15 min at 80 °C in the oven. The control layer was created by pouring another mixture of PDMS (5:1 w/w elastomer/curing agent) on the respective structured silicon wafer to create a 5 μm thick layer of structured PDMS. The control layer was then precured for 30 min at 80 °C in an oven, and connection holes were punched afterward (biopsy puncher, Miltex, 1 mm o.d.). The two PDMS layers were aligned and cured overnight at 80 °C in the oven to achieve a permanent and final bonding. Next, holes were punched (biopsy puncher, Miltex, 1 mm o.d.) through the two PDMS layers in order to create the fluidic connections to the fluidic layer, and the resulting multilayer PDMS assembly was then plasma-bonded to a glass coverslip (24 × 60 mm No. 5, Menzel Gläser) using a plasma cleaner (PDC-32G plasma cleaner, Harrick Plasma, power 18 W, time 45 s).

Patterning of Pt Electrodes. For electrical characterization of AgTCNQ and AuTTF wires, platinum patterned electrodes were fabricated on top of glass coverslips (24 × 60 mm No. 1, Menzel Gläser) by conventional photolithographic methods and physical vapor deposition. Briefly, after dehydration of the glass coverslips for 5 min at 180 °C, a layer of image reversal photoresist AZ5214E (AZ Electronic Materials) was spin-coated on the slips at 4000 rpm for 30 s. After a soft bake for 1 min at 100 °C, the glass coverslip was exposed to 75 mJ/cm^2 UV light (at 405 nm) using a mask aligner (MA-6 mask aligner, Karl Süss) and a transparency photomask (JD Photo-Tools). Next, the glass coverslip was baked for 45 s at 120 °C and again exposed to 300 mJ/cm^2 UV light (405 nm) using a mask aligner. After development in AZ726 developer (AZ Electronic Materials) a 10 nm adhesion layer of chromium and a 100 nm layer of platinum were deposited on the glass cover by physical vapor deposition (Plassys II, Plassys-Bestek). Finally the surplus metal was removed by Microposit Remover 1165 (Rohm and Haas), resulting in the patterned electrode slides.

Different designs were fabricated for two- and four-point electrical characterization (Supporting Information Figure S1).

Chemicals. Solutions of tetrathiafulvalene (purchased from Acros Organics, concentration 24 mM), hydrogen tetrachloroaurate (purchased from Sigma−Aldrich, concentration 6 mM), and tetracyanoquinodimethane (purchased from Fluka, saturated solution) were prepared in acetonitrile. 1,4-Bis(imidazol-1-ylmethyl)benzene was synthesized as described by Dhal *et al.*,[63] and a 20 mM (bix) solution in ethanol was used in our experiments with a 20 mM aqueous solution of zinc nitrate hexahydrate ($Zn(NO_3)\cdot 6H_2O$), purchased from Merck.

Electroless-Deposited Silver Film. The silver films were fabricated using commercial HE-300 solutions (Peacock Laboratories, Inc.). Two precursor solutions were prepared for the electroless deposition of silver; one contained a 1:1 mixture of the activator and the silver solution, and the other solution contained the reducing agent. The mixture and reducer solution were diluted by a factor of 2 and 3, respectively, with deionized water from stock solutions. Different concentrations of the two precursor solutions were studied; however an additional dilution with deionized water by a factor of 3 of the two precursor solutions was always used in our experiments, unless otherwise indicated.

Characterization of Nanomaterials. *Four-Point Measurements.* The electrical measurements were performed by a applying

current through a source electrode pair and monitoring the resulting potential using a sensing electrode pair (Keithley 2612A). The macroscopic electrodes were positioned onto the end of the Pt electrodes with a micromanipulator.

SEM, EDX, PXRD, and ATR-IR. SEM images and energy dispersive X-ray spectroscopy were obtained using a FEI Quanta 200 FEG. The powder X-ray diffraction measurements were collected using a Stoe STADIP powder diffractometer equipped with a linear position-sensitive detector. Samples were loaded into 0.3 mm diameter capillary tubes (Merck) before PXRD measurement. Attenuated total reflectance IR spectra were recorded using a FTIR spectrophotometer (Perkin-Elmer, Spectrum 100) equipped with an ATR unit (Specac).

Conflict of Interest: The authors declare no competing financial interest.

Acknowledgment. Funding from the Swiss National Science Foundation (grant no. 200021_134829/1) and the European Research Council (ERC Starting Grant no. 203428 and 7th Framework Programme for Research and Technology, project no. CP-FP 213803-2 ROC) is gratefully acknowledged. We thank Phillip Kuhn for the support with the microfabrication, Dr. Michael Wöhrle for the XRD measurements, and Tom Robinson for discussion and proofreading of the manuscript. Furthermore, we are thankful for use of the clean room facility (FIRST) and the Electron Microscopy Center (EMEZ) of ETH.

Supporting Information Available: This section includes a movie illustrating the diffusive mixing condition of the device, micrographs of the device, and additional information clarifying AgTCNQ and AuTTF wire growth. Moreover, SEM images, EDX and ATR-IR spectra, and PXRD patterns of the structures presented are included. This material is available free of charge *via* the Internet at http://pubs.acs.org.

REFERENCES AND NOTES

1. Adam, D.; Schuhmacher, P.; Simmerer, J.; Häussling, L.; Siemensmeyer, K.; Etzbachi, K. H.; Ringsdorf, H.; Haarer, D. Fast Photoconduction in the Highly Ordered Columnar Phase of a Discotic Liquid Crystal. *Nature* **1994**, *371*, 141–143.
2. Sundar, V. C.; Zaumseil, J.; Podzorov, V.; Menard, E.; Willett, R. L.; Someya, T.; Gershenson, M. E.; Rogers, J. A. Elastomeric Transistor Stamps: Reversible Probing of Charge Transport in Organic Crystals. *Science* **2004**, *303*, 1644–1646.
3. Mas-Torrent, M.; Hadley, P.; Bromley, S. T.; Ribas, X.; Tarrés, J.; Mas, M.; Molins, E.; Veciana, J.; Rovira, C. Correlation between Crystal Structure and Mobility in Organic Field-Effect Transistors Based on Single Crystals of Tetrathiafulvalene Derivatives. *J. Am. Chem. Soc.* **2004**, *126*, 8546–8553.
4. Yang, X.; Loos, J.; Veenstra, S. C.; Verhees, W. J. H.; Wienk, M. M.; Kroon, J. M.; Michels, M. A. J.; Janssen, R. A. J. Nanoscale Morphology of High-Performance Polymer Solar Cells. *Nano Lett.* **2005**, *5*, 579–583.
5. Chang, J.; Sun, B.; Breiby, D.; Nielsen, M.; Solling, T.; Giles, M.; McCulloch, I.; Sirringhaus, H. Enhanced Mobility of Poly(3-hexylthiophene) Transistors by Spin-Coating from High-Boiling-Point Solvents. *Chem. Mater.* **2004**, *16*, 4772–4776.
6. Bissell, R.; Córdova, E.; Kaifer, A.; Stoddart, J. A Chemically and Electrochemically Switchable Molecular Shuttle. *Nature* **1994**, *369*, 133–137.
7. Huang, Y.; Duan, X.; Cui, Y.; Lauhon, L. J.; Kim, K. H.; Lieber, C. M. Logic Gates and Computation from Assembled Nanowire Building Blocks. *Science* **2001**, *294*, 1313–1317.
8. Browne, W. R.; Feringa, B. L. Making Molecular Machines Work. *Nat. Nanotechnol.* **2006**, *1*, 25–35.
9. Neufeld, A. K.; O'Mullane, A. P.; Bond, A. M. Control of Localized Nanorod Formation and Patterns of Semiconducting CuTCNQ Phase I Crystals by Scanning Electrochemical Microscopy. *J. Am. Chem. Soc.* **2005**, *127*, 13846–13853.
10. Cao, G.; Ye, C.; Fang, F.; Xing, X.; Xu, H.; Sun, D.; Chen, G. Crystalline Quasi-One-Dimensional Ag−TCNQ Micro/Nanostructures Synthesized by Solution Reaction. *Mater. Sci. Eng., B* **2005**, *119*, 41–45.
11. Cao, G.; Fang, F.; Ye, C.; Xing, X.; Xu, H.; Sun, D.; Chen, G. Microscopy Investigation of Ag-TCNQ Micro/Nanostructures Synthesized *via* Two Solution Routes. *Micron* **2005**, *36*, 285–290.
12. Naka, K.; Ando, D.; Wang, X.; Chujo, Y. Synthesis of Organic-Metal Hybrid Nanowires by Cooperative Self-Organization of Tetrathiafulvalene and Metallic Gold *via* Charge-Transfer. *Langmuir* **2007**, *23*, 3450–3454.
13. ÒMullane, A. P.; Fay, N.; Nafady, A.; Bond, A. M. Preparation of Metal−TCNQ Charge-Transfer Complexes on Conducting and Insulating Surfaces by Photocrystallization. *J. Am. Chem. Soc.* **2007**, *129*, 2066–2073.
14. Zheng, W.; Li, Z.; Yang, F.; Song, X.; Zhang, H.; Liu, Y.; Wang, C. A Simple and Effective Route for One-Dimensional Ag-TCNQ Metal-Organic Microstructures. *Mater. Lett.* **2008**, *62*, 1448–1450.
15. Fan, Z. Y.; Mo, X. L.; Chen, G. R.; Lu, J. G. Synthesis, Morphology and Electrical Characterization of Ag-TCNQ from Thin Film to Nanowire. *Rev. Adv. Mater. Sci.* **2003**, *5*, 72–75.
16. Xiao, J.; Yin, Z.; Wu, Y.; Guo, J.; Cheng, Y.; Li, H.; Huang, Y.; Zhang, Q.; Ma, J.; Boey, F.; *et al.* Chemical Reaction between Ag Nanoparticles and TCNQ Microparticles in Aqueous Solution. *Small* **2011**, *7*, 1242–1246.
17. Ye, C.; Cao, G.; Fang, F.; Xu, H.; Xing, X.; Sun, D.; Chen, G. Morphology Investigation of Ag(TCNQ) Synthesized by the Vapor-Transport Reaction Method. *Micron* **2005**, *36*, 461–464.
18. Liu, S.; Wang, W. M.; Briseno, A. L.; Mannsfeld, S. C. B.; Bao, Z. Controlled Deposition of Crystalline Organic Semiconductors for Field-Effect-Transistor Applications. *Adv. Mater.* **2009**, *21*, 1217–1232.
19. Hoffman, R. C.; Potember, R. S. Organometallic Materials for Erasable Optical Storage. *Appl. Opt.* **1989**, *28*, 1417–1421.
20. Xiao, K.; Tao, J.; Puretzky, A. A.; Ivanov, I. N.; Retterer, S. T.; Pennycook, S. J.; Geohegan, D. B. Selective Patterned Growth of Single-Crystal Ag-TCNQ Nanowires for Devices by Vapor-Solid Chemical Reaction. *Adv. Funct. Mater.* **2008**, *18*, 3043–3048.
21. Ji, Z.; Li, H.; Liu, Y.; Hu, W. Electroplating Silver Tetracyanoquinodimethane between Gold Micro-Gap Electrodes for the Fabrication of Coplanar Devices, a New Way to Integrate Material Synthesis and Devices Fabrication within One Step. *Appl. Phys. A: Mater. Sci. Process.* **2008**, *91*, 301–303.
22. Briseno, A. L.; Mannsfeld, S. C. B.; Ling, M. M.; Liu, S.; Tseng, R. J.; Reese, C.; Roberts, M. E.; Yang, Y.; Wudl, F.; Bao, Z. Patterning Organic Single-Crystal Transistor Arrays. *Nature* **2006**, *444*, 913–917.
23. Carbonell, C.; Imaz, I.; Maspoch, D. Single-Crystal Metal-Organic Framework Arrays. *J. Am. Chem. Soc.* **2011**, *133*, 2144–2147.
24. Piner, R. D.; Zhu, J.; Xu, F.; Hong, S.; Mirkin, C. A. "Dip-Pen" Nanolithography. *Science* **1999**, *283*, 661–663.
25. Liu, X.; Zhang, Y.; Goswami, D. K.; Okasinski, J. S.; Salaita, K.; Sun, P.; Bedzyk, M. J.; Mirkin, C. A. The Controlled Evolution of a Polymer Single Crystal. *Science* **2005**, *307*, 1763–1766.
26. Dendukuri, D.; Pregibon, D. C.; Collins, J.; Hatton, T. A.; Doyle, P. S. Continuous-Flow Lithography for High-Throughput Microparticle Synthesis. *Nat. Mater.* **2006**, *5*, 365–369.
27. Edel, J.; Fortt, R.; deMello, J.; deMello, A. Microfluidic Routes to the Controlled Production of Nanoparticles. *Chem. Commun.* **2002**, 1136–1137.
28. Dittrich, P. S.; Heule, M.; Renaud, P.; Manz, A. On-Chip Extrusion of Lipid Vesicles and Tubes through Microsized Apertures. *Lab Chip* **2006**, *6*, 488–493.
29. Pumera, M. Nanomaterials Meet Microfluidics. *Chem. Commun.* **2011**, *47*, 5671–5680.
30. Puigmartí-Luis, J.; Rubio-Martínez, M.; Hartfelder, U.; Imaz, I.; Maspoch, D.; Dittrich, P. S. Coordination Polymer Nanofibers

Generated by Microfluidic Synthesis. *J. Am. Chem. Soc.* **2011**, *133*, 4216–4219.
31. Khoo, H. S.; Lin, C.; Huang, S.-H.; Tseng, F.-G. Self-Assembly in Micro- and Nanofluidic Devices: A Review of Recent Efforts. *Micromachines* **2011**, *2*, 17–48.
32. Wang, Z.; Bao, R.; Zhang, X.; Ou, X.; Lee, C.-S.; Chang, J. C.; Zhang, X. One-Step Self-Assembly, Alignment, and Patterning of Organic Semiconductor Nanowires by Controlled Evaporation of Confined Microfluids. *Angew. Chem., Int. Ed.* **2011**, *50*, 2811–2815.
33. Kenis, P.; Ismagilov, R.; Whitesides, G. Microfabrication Inside Capillaries Using Multiphase Laminar Flow Patterning. *Science* **1999**, *285*, 83–85.
34. Puigmartí-Luis, J.; Schaffhauser, D.; Burg, B. R.; Dittrich, P. S. A Microfluidic Approach for the Formation of Conductive Nanowires and Hollow Hybrid Structures. *Adv. Mater.* **2010**, *22*, 2255–2259.
35. Jahn, A.; Vreeland, W. N.; Gaitan, M.; Locascio, L. E. Controlled Vesicle Self-Assembly in Microfluidic Channels with Hydrodynamic Focusing. *J. Am. Chem. Soc.* **2004**, *126*, 2674–2675.
36. Hou, S.; Wang, S.; Yu, Z. T. F.; Zhu, N. Q. M.; Liu, K.; Sun, J.; Lin, W.-Y.; Shen, C. K. F.; Fang, X.; Tseng, H.-R. A Hydrodynamically Focused Stream as a Dynamic Template for Site-Specific Electrochemical Micropatterning of Conducting Polymers. *Angew. Chem., Int. Ed.* **2008**, *120*, 1088–1091.
37. Witters, D.; Vergauwe, N.; Ameloot, R.; Vermeir, S.; De Vos, D.; Puers, R.; Sels, B.; Lammertyn, J. Digital Microfluidic High-Throughput Printing of Single Metal-Organic Framework Crystals. *Adv. Mater.* **2012**, *24*, 1316–1320.
38. Du, W.; Li, L.; Nichols, K. P.; Ismagilov, R. F. SlipChip. *Lab Chip* **2009**, *9*, 2286–2292.
39. Li, L.; Du, W.; Ismagilov, R. F. Multiparameter Screening on SlipChip Used for Nanoliter Protein Crystallization Combining Free Interface Diffusion and Microbatch Methods. *J. Am. Chem. Soc.* **2010**, *132*, 112–119.
40. Zheng, B.; Roach, L. S.; Ismagilov, R. F. Screening of Protein Crystallization Conditions on a Microfluidic Chip Using Nanoliter-Size Droplets. *J. Am. Chem. Soc.* **2003**, *125*, 11170–11171.
41. Theberge, A. B.; Courtois, F.; Schaerli, Y.; Fischlechner, M.; Abell, C.; Hollfelder, F.; Huck, W. T. S. Microdroplets in Microfluidics: An Evolving Platform for Discoveries in Chemistry and Biology. *Angew. Chem., Int. Ed.* **2010**, *49*, 5846–5868.
42. Ho, Y.-P.; Grigsby, C. L.; Zhao, F.; Leong, K. W. Tuning Physical Properties of Nanocomplexes through Microfluidics-Assisted Confinement. *Nano Lett.* **2011**, *11*, 2178–2182.
43. Unger, M. A.; Chou, H. P.; Thorsen, T.; Scherer, A.; Quake, S. R. Monolithic Microfabricated Valves and Pumps by Multilayer Soft Lithography. *Science* **2000**, *288*, 113–116.
44. Hansen, C. L.; Skordalakes, E.; Berger, J. M.; Quake, S. R. A Robust and Scalable Microfluidic Metering Method that Allows Protein Crystal Growth by Free Interface Diffusion. *Proc. Natl. Acad. Sci. U. S. A.* **2002**, *99*, 16531–16536.
45. Hansen, C. L.; Classen, S.; Berger, J. M.; Quake, S. R. A Microfluidic Device for Kinetic Optimization of Protein Crystallization and *in Situ* Structure Determination. *J. Am. Chem. Soc.* **2006**, *128*, 3142–3143.
46. Imaz, I.; Hernando, J.; Ruiz-Molina, D.; Maspoch, D. Metal-Organic Spheres as Functional Systems for Guest Encapsulation. *Angew. Chem., Int. Ed.* **2009**, *48*, 2325–2329.
47. Gao, Y.; Chen, L. Versatile Control of Multiphase Laminar Flow for In-Channel Microfabrication. *Lab Chip* **2008**, *8*, 1695–1699.
48. Mukherjee, B.; Mukherjee, M.; Sim, K.; Pyo, S. Solution Processed, Aligned Arrays of TCNQ Micro Crystals for Low-Voltage Organic Phototransistor. *J. Mater. Chem.* **2011**, *21*, 1931–1936.
49. Tu, D.; Wang, C.; Ji, Z.; Hu, W.; Liu, M. Fabrication and Electrical Characteristics of AgTCNQ Crossbar Switches for Organic Molecular Memories and Logics. *IEEE Conf. Electron Devices Solid-State Circuits* **2005**, 575–578.
50. Fan, Z.; Wang, D.; Lu, J.; Mo, X. Silver-Tetracyanoquinodimethane (Ag-TCNQ) Nanostructures and Nanodevice. *IEEE-Nano* **2003**, *2*, 588–591.
51. Ren, L.; Fu, L.; Liu, Y.; Chen, S.; Liu, Z. Electrochemical Synthesis of High-Quality AgTCNQ Nanowires Using Carbon Nanotube Electrodes. *Adv. Mater.* **2009**, *21*, 4742–4746.
52. Chen, X.; Zheng, G.; Cutler, J. I.; Jang, J.-W.; Mirkin, C. A. In-Wire Conversion of a Metal Nanorod Segment into an Organic Semiconductor. *Small* **2009**, *5*, 1527–1530.
53. Xiao, K.; Tao, J.; Pan, Z.; Puretzky, A. A.; Ivanov, I. N.; Pennycook, S. J.; Geohegan, D. B. Single-Crystal Organic Nanowires of Copper-Tetracyanoquinodimethane: Synthesis, Patterning, Characterization, and Device Applications. *Angew. Chem., Int. Ed.* **2007**, *46*, 2650–2654.
54. O'Kane, S. New Crystalline Polymers of Ag(TCNQ) and Ag(TCNQF$_4$): Structures and Magnetic Properties. *J. Solid State Chem.* **2000**, *152*, 159–173.
55. Liu, H.; Zhao, Q.; Li, Y.; Liu, Y.; Lu, F.; Zhuang, J.; Wang, S.; Jiang, L.; Zhu, D.; Yu, D.; *et al.* Field Emission Properties of Large-Area Nanowires of Organic Charge-Transfer Complexes. *J. Am. Chem. Soc.* **2005**, *127*, 1120–1121.
56. Chen, Z.; Lu, C. Humidity Sensors: A Review of Materials and Mechanisms. *Sensor Lett.* **2005**, *3*, 274–295.
57. Kulwicki, B. M. Humidity Sensors. *J. Am. Ceram. Soc.* **1991**, *74*, 697–708.
58. Li, Z.; Zhang, H.; Zheng, W.; Wang, W.; Huang, H.; Wang, C.; MacDiarmid, A. G.; Wei, Y. Highly Sensitive and Stable Humidity Nanosensors Based on LiCl Doped TiO_2 Electrospun Nanofibers. *J. Am. Chem. Soc.* **2008**, *130*, 5036–5037.
59. Chiang, J.; MacDiarmid, A. "Polyaniline": Protonic Acid Doping of the Emeraldine form to the Metallic Regime. *Synth. Met.* **1986**, *13*, 193–205.
60. Braun, D.; Heeger, A. J. Visible Light Emission from Semiconducting Polymer Diodes. *Appl. Phy. Lett.* **1991**, *58*, 1982–1984.
61. Sakai, Y.; Sadaoka, Y.; Matsuguchi, M. Humidity Sensors Based on Polymer Thin Films. *Sens. Actuators, B* **1996**, 85–90.
62. Katz, H. E.; Hong, X. M.; Dodabalapur, A.; Sarpeshkar, R. Organic Field-Effect Transistors with Polarizable Gate Insulators. *J. Appl. Phy.* **2002**, *91*, 1572–1576.
63. Dhal, P. K.; Arnold, F. H. Metal-Coordination Interactions in the Template-Mediated Synthesis of Substrate-Selective Polymers: Recognition of Bis(imidazole) Substrates by Copper(II)iminodiacetate Containing Polymers. *Macromolecules* **1992**, *25*, 7051–7059.